applied sciences

MDPI

Article

Convolutional Neural Network for Interface Defect Detection in Adhesively Bonded Dissimilar Structures

Damira Smagulova [1,2], Vykintas Samaitis [1] and Elena Jasiuniene [1,2,*]

[1] Prof. K. Barsauskas Ultrasound Research Institute, Kaunas University of Technology, K. Barsausko Str. 59, LT-51423 Kaunas, Lithuania; damira.smagulova@ktu.lt (D.S.); vykintas.samaitis@ktu.lt (V.S.)
[2] Department of Electronics Engineering, Faculty of Electrical and Electronic Engineering, Kaunas University of Technology, Studentu Str. 50, LT-51368 Kaunas, Lithuania
* Correspondence: elena.jasiuniene@ktu.lt; Tel.: +370-698-00899

Abstract: This study presents an ultrasonic non-destructive method with convolutional neural networks (CNN) used for the detection of interface defects in adhesively bonded dissimilar structures. Adhesive bonding, as the weakest part of such structures, is prone to defects, making their detection challenging due to various factors, including surface curvature, which causes amplitude variations. Conventional non-destructive methods and processing algorithms may be insufficient to enhance detectability, as some influential factors cannot be fully eliminated. Even after aligning signals reflected from the sample surface and interface, in some cases, due to non-parallel interfaces, persistent amplitude variations remain, significantly affecting defect detectability. To address this problem, a proposed method that integrates ultrasonic NDT and CNN, and which is able to recognize complex patterns and non-linear relationships, is developed in this work. Traditional ultrasonic pulse-echo testing was performed on adhesive structures to collect experimental data and generate C-scan images, covering the time gate from the first interface reflection to the time point where the reflections were attenuated. Two classes of datasets, representing defective and defect-free areas, were fed into the neural network. One subset of the dataset was used for model training, while another subset was used for model validation. Additionally, data collected from a different sample during an independent experiment were used to evaluate the generalization and performance of the neural network. The results demonstrated that the integration of a CNN enabled high prediction accuracy and automation of the analysis process, enhancing efficiency and reliability in detecting interface defects.

Keywords: convolutional neural network; detectability; automatization; adhesive joints; ultrasonic; dissimilar materials

Citation: Smagulova, D.; Samaitis, V.; Jasiuniene, E. Convolutional Neural Network for Interface Defect Detection in Adhesively Bonded Dissimilar Structures. *Appl. Sci.* **2024**, *14*, 10351. https://doi.org/10.3390/app142210351

Academic Editor: Rui Araújo

Received: 4 October 2024
Revised: 18 October 2024
Accepted: 30 October 2024
Published: 11 November 2024

1. Introduction

Adhesive-bonded structures have attracted considerable interest in the aerospace, marine, automotive, civil and other industries due to their cost-effectiveness and superior performance characteristics. The advantages of these structures include even load distribution, reduced weight, the ability to bond dissimilar materials, high strength/weight ratios, and improved fatigue life, impact resistance, and residual strength [1–3]. In the aerospace sector, for example, weight reduction is especially valuable, as it contributes to lower CO_2 emissions, enhanced aircraft performance, and greater cost efficiency. The use and popularity of lightweight materials compared to metal alloys has increased significantly in aviation, aerospace, and motorsports due to their efficiency [4]. In modern aircraft models, such as the Airbus A350XWB, carbon fiber accounts for 50% of the total weight, an increase of 30% compared to the earlier A380 model [5].

Nevertheless, the integrity of adhesively bonded structures can be compromised by external loadings, aging, and environmental conditions, which can lead to the forming of various defects [1]. Common defects to which adhesive joints are prone include interface

defects such as delaminations, debonding, porosity, and voids [6]. These defects are often invisible and can result in catastrophic failures if undetected. Therefore, regular application of reliable non-destructive testing (NDT) methods is crucial for monitoring the mechanical properties and structural integrity of adhesive joints [7–9].

Various NDT methods can be applied for the inspection of adhesive joints, including thermography [10], ultrasound [11,12], guided waves [6], eddy current [13], and X-ray radiography. These methods do not affect the performance of the structure and can provide valuable information regarding the presence, quantity, location, size, and type of defects [11]. The selection of a particular NDT technique depends on the inspection requirements, as each technique has its advantages and limitations. For example, radiography is effective in detecting porosity, voids, and inclusions and providing accurate information on the location of defects, but is expensive and involves exposure to radiation. Thermography is non-contact and can quickly inspect large areas, making it suitable for detecting surface defects, but its effectiveness decreases with depth, making it less reliable for detecting subsurface defects. Eddy current testing is sensitive to small surface cracks and corrosion and works well with conductive materials, but has limited depth penetration. Ultrasound, on the other hand, can detect both surface and subsurface defects, making it versatile, but requires skilled operators and direct contact with the surface. Guided waves can inspect large areas efficiently, especially in complex structures, but are sensitive to environmental noise and may require signal interpretation [14]. Therefore, the selection of suitable techniques depends on the object structure and inspection requirements.

Despite the wide range of NDT techniques available, the detection of interface defects in adhesive joints remains challenging [15]. This is particularly true in cases where surface curvature causes amplitude variations in ultrasonic testing, making defect detection less reliable [16].

Recent advances, such as the use of ultrasonic guided waves and post-processing algorithms, have attempted to improve the detectability of defects in multilayered structures. Techniques such as the generation of A0 mode ultrasonic guided waves, the weighted root mean square (WRMS) processing algorithm, and other optimization techniques have demonstrated improved accuracy by correlating wave properties with the presence of interface defects [17–19]. Solodov et al. [7] investigated zero-volume kissing bonds using both linear and non-linear ultrasonic testing. Their findings showed that high nonlinearity corresponded to weaker bond strength, while lower nonlinearity indicated stronger bonds. Linear ultrasonic testing was effective in identifying only significant reductions in bond strength [7]. Yilmaz et al. [18] compared the performance of air-coupled, contact, and immersion ultrasonic techniques for evaluating bonding quality using both bulk and guided waves. Their study found that bulk waves performed best overall, while guided waves were more effective at detecting the presence of defects than at sizing them [20]. In addition, various data processing algorithms have been developed to enhance detectability and reliability, such as data fusion techniques combining results from multiple NDT methods [2,21], the self-interference cancellation algorithm, which eliminates multiple reflection waveforms in the echoed signal [22], and the density-based spatial clustering of applications with noise (DBSCAN) algorithm, which is used for pattern analysis of extracted ultrasonic guided wave features in order to identify delaminations [23]. In one study, extensive research into adhesive bonds and the evaluation of bond quality, with a focus on increasing reliability and detection probability by eliminating influencing factors such as surface and interface curvature through post-processing algorithms, was performed [16]. This work included analysis of higher order interface reflections, extraction of amplitude ratio coefficients from C-scan images for selected time windows, and time alignment of signals reflected from object surface and interface [16]. In our recent studies, we have extracted different ultrasonic features and evaluated their performance for comparison [3]. All of these efforts have resulted in an improvement in defect detectability and sizing.

Machine learning (ML), artificial intelligence (AI), and deep learning are increasingly being integrated into NDT technologies, offering more accurate and automated inspec-

tion systems [4]. Traditional NDT methods are often based on a manual extraction of the features, which does not allow capture of all the different features within the data, and as a result, features can be missed. In contrast, AI/ML methods, such as neural networks, can automatically learn features and relationships from the data, improving defect detection [11,24,25]. In addition to machine learning techniques, alternative methods such as fuzzy logic-based approaches, which handle uncertainties in defect detection by grouping similar defect maps into classes despite inherent fuzziness in the data, can be applied for defect classification, particularly in materials with complex subsurface properties like carbon fiber-reinforced polymers (CFRP) [26].

Recent studies have demonstrated improvements in defect detection through the application of AI/ML methods. For example, Wang et al. [27] provided a comprehensive review of the application of artificial intelligence (AI) and machine learning (ML) techniques throughout the entire life cycle of high-performance composites, including design, manufacturing, testing, and monitoring. The integration of AI/ML aids in material development, process optimization, property prediction, and damage diagnosis [27]. Chen et al. [11] in a recent work proposed enhancements to the baseline YOLOv8 deep learning method for improving defect detection in phased array ultrasonic testing (PAUT) in low-resolution images. Standard strided convolution was replaced with space-to-depth convolution (SPD-Conv) to reduce information loss and introduce a bi-level routing and spatial attention (BRSA) module to generate multiscale feature maps with richer details. The enhanced algorithm achieved significant improvements in detecting challenging defects, such as side-drilled holes (SDH) and flat bottom holes (FBH) in aluminum block samples [11]. Although there has been limited research specifically addressing adhesive joints and interface defects, some notable efforts exist. For example, Rao et al. [1] proposed an ultrasonic inversion method using a supervised fully convolutional network (FCN) for quantitative reconstruction of high-contrast defects hidden within multilayered composite materials. This method accurately reconstructed L-wave velocity models of defects and demonstrated potential for online detection of adhesively bonded composites [1]. Tenreiro et al. [24] described ML algorithm development approaches such as kNN, naive Bayes classifier, random forest, and gradient booster for monitoring single-lap adhesive joints for weak adhesion and voids by extracting predominant features from Lamb waves [24]. In our recent work, Smagulova et al. [28], the automated technique of the ultrasonic method combined with machine learning algorithms was presented for detection and classification of the depth of interface defects in adhesive joints. A support vector machine (SVM) was trained with prepared datasets, demonstrating high prediction accuracy and the ability to classify defect depth in adhesive joints [28].

This paper focuses on the study of ultrasonic waves for detecting interface defects in adhesive joints, with the use of post-processing algorithms to improve detectability and reliability, and the application of modern deep learning techniques, specifically convolutional neural networks. The aim of this study was to develop and optimize an ultrasonic non-destructive testing (NDT) method integrated with convolutional neural networks (CNN) to improve the detection of interface defects in bonded structures and to automate the process. Considering the challenges posed by surface curvature and other factors that cannot be fully eliminated by conventional ultrasonic NDT techniques and post-processing algorithms that limit the accuracy of interface defect detection, the proposed approach can improve the detection accuracy by exploiting the pattern recognition and non-linear relationship capabilities of CNN. In order to achieve this goal, ultrasonic pulse-echo testing was performed on aluminum adhesively bonded to composite structures to collect data for further generation of C-scan images. Datasets were prepared by classifying experimental data into defective and not defective areas. The CNN was trained with a data subset to recognize patterns and features of images. The other data subset was used for CNN validation. In addition, the generalization ability of the trained model was evaluated using data collected from another sample with interface defects where the curvature was not visible

and also affected detection. The performance of the developed technique was evaluated and compared.

2. Materials and Methods

This section describes the methodology used to develop an ultrasonic NDT technique integrated with CNN for the detection of interface defects in adhesively bonded materials. The technique is designed to analyze complex C-scan images, where amplitude variations are caused not only by defects, but also by surface curvature, and therefore create challenges in defect detection. The workflow includes data acquisition using an ultrasonic pulse-echo technique, followed by post-processing to align all signals to the surface reflection time, reducing the impact of surface curvature on defect detectability. Further, the generation of C-scans for problem analysis, data preparation, and the training, validation, and generalization of the CNN model to classify defective and non-defective regions was performed. The overall workflow is illustrated in Figure 1.

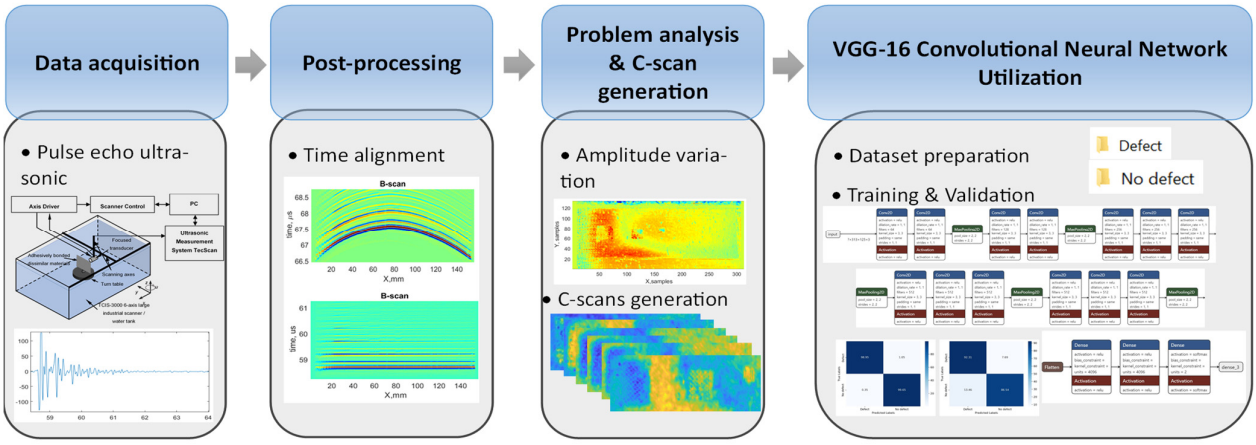

Figure 1. Schematic of the workflow of ultrasonic NDT integrated with CNN.

2.1. Object Description

The objects examined in this study consisted of aluminum bonded to carbon fiber-reinforced plastic (CFRP), manufactured by COTESA GmBH, Mittweida, Germany, and FL Technics, a global aircraft maintenance and repair company based in Kaunas, Lithuania. These structures simulated typical aerospace industry components. The adhesive joints were formed using two layers of structural adhesive films, Scotch Weld AF163-2K. Both samples had three disbond defects placed between the adhesive films. The defects, rectangular in shape, had dimensions of 15 × 15 mm, 10 × 10 mm, and 5 × 5 mm. A double-folded release film (A5000RED) was used to create the disbond-type defects. Schematics of both samples are shown in Figure 2. Sample No.1 consisted of a 1.6 mm thick aluminum plate and a 5.11 mm thick CFRP plate, while Sample No.2 had a 1.82 mm thick aluminum plate and a 1.6 mm thick CFRP plate. The adhesive thickness was 0.22 mm for Sample No.1 and 0.18 mm for Sample No.2.

2.2. Ultrasonic Inspection and Problematic

Ultrasonic pulse-echo inspections were performed on both samples in immersion mode to gather experimental data. An automated TecScan system was used for the measurements, with focused transducers of 10 MHz and 15 MHz applied to Sample No.1 and Sample No.2, respectively. Each sample was immersed in a water tank, where the alignment between the sample surface and the transducer beam was carefully adjusted. The scanning was performed along the y and z directions from the aluminum side of the samples. The experimental set-up is shown in Figure 3.

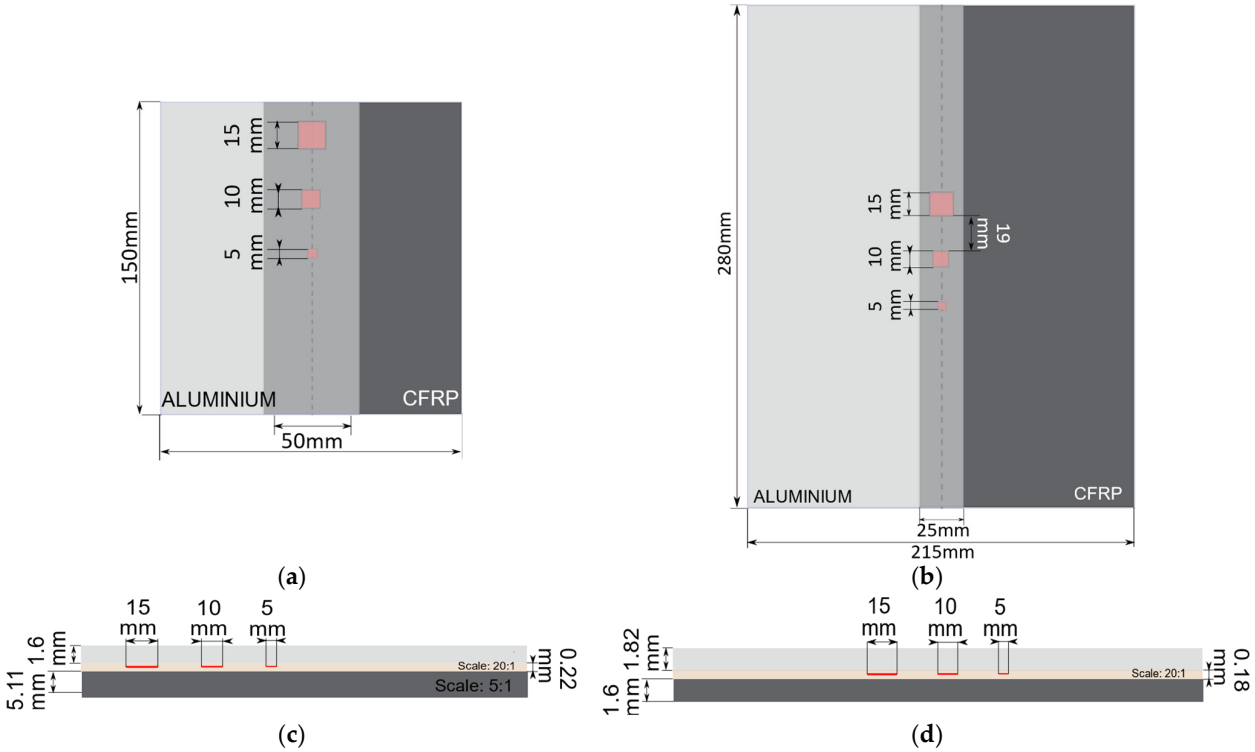

Figure 2. Top and side view of adhesively bonded aluminum to CFRPs. (**a**) Top view of Sample No.1; (**b**) top view of Sample No.2; (**c**) side view of Sample No.1; (**d**) side view of Sample No.2.

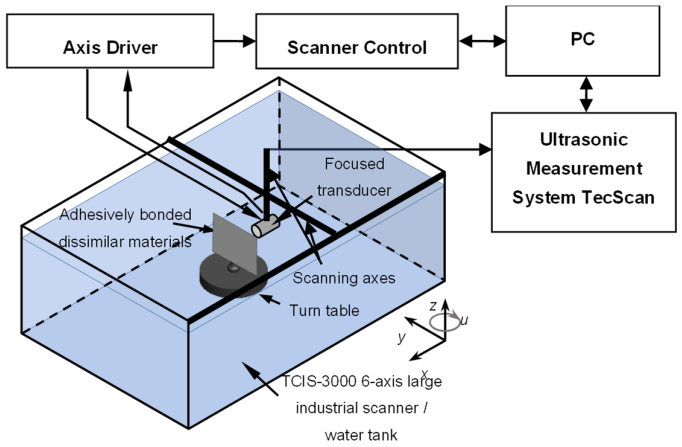

Figure 3. Experimental set-up.

The experimental data collected were analyzed using the MatLab R2023a program. The curvature of the two samples, which was not observed visually, was clearly detected for both samples during the measurement and analysis. For example, in the case of Sample No.1, the approximate time difference between the earliest and latest reflections received by the transducer reached 0.5 µs due to the influence of the curvature. However, such a small time difference has a huge impact on the detection of interface defects. In order to reduce the influence of curvature and improve the detection of interface defects, the post-processing time alignment algorithm described in our previous work [16] was applied to the collected data. This algorithm aligned all signals based on the time of ultrasonic wave reflections from the sample surface. As a result, detection was improved. In the case of sample No.1, the largest defect became clearly visible on the ultrasonic C-scan (Figure 4b), while the barely distinguished shapes of the two smaller defects could hardly

be observed. Additional C-scans were generated for time intervals corresponding to three repeated reflections from the interface, and are shown in Figure 4c,d.

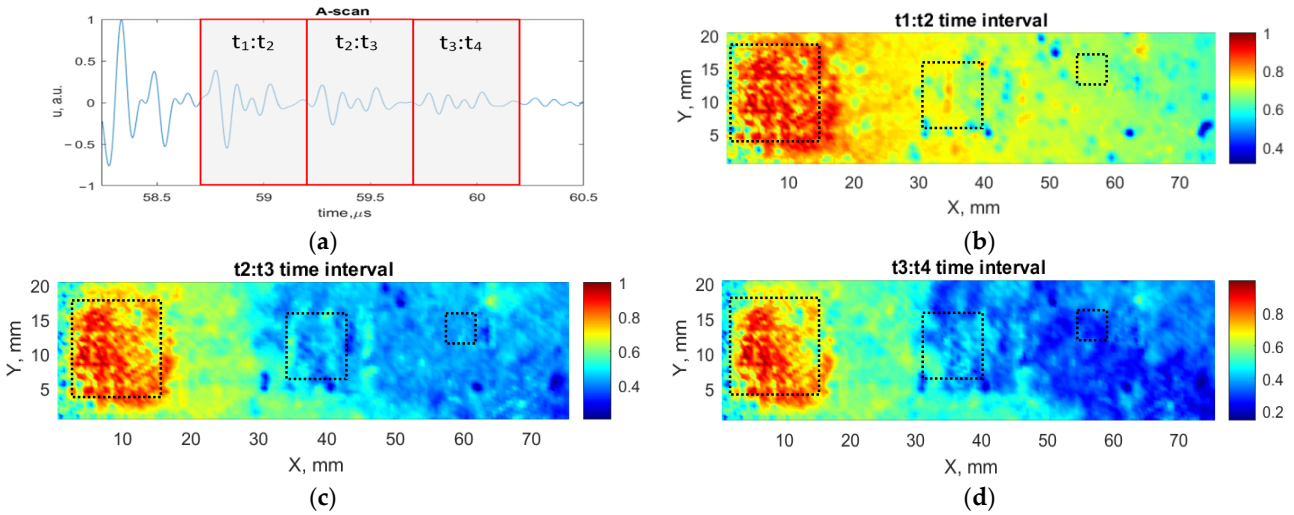

Figure 4. A-scan and C-scans of multiple reflections from the Sample No.1 interface. (**a**) A-scan with shown selected time intervals of 3 multiple interface reflections; (**b**) C-scan at t_1:t_2 time interval; (**c**) C-scan at t_2:t_3 time interval; (**d**) C-scan at t_3:t_4 time interval. Dash boxes show the position of the defects.

While defects could be visually distinguished on the C-scans, consistent amplitude variations across the sample interface made it impossible to reliably identify defects based on amplitude during data analysis. This pattern of amplitude variations has a systematic behavior across ultrasonic C-scans. Thus, despite time alignment technique, these amplitude fluctuations across the scan persisted, and the reason for this could be the complex interaction of factors that affected how the ultrasonic waves were received at different points on the surface. The possible reasons for the observed amplitude variations could include changes in the angle at which ultrasonic waves interacted with the materials and reflected from the interface, affecting both the intensity of the reflected wave and the time-of-flight. Additional factors such as wave interference and reverberation may also have contributed to these variations. While amplitude variations due to sample curvature effects complicated the detection of interface defects, manually and randomly picked up samples along the time axis revealed that certain scans could clearly display all three defects, either in the same or different amplitude contrast phases (see Figure 5).

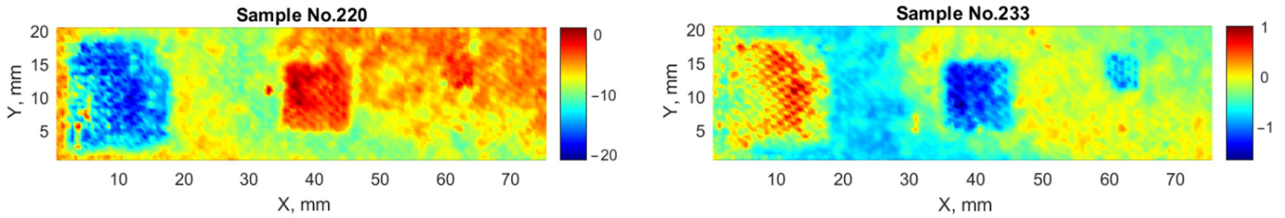

Figure 5. C-scans at specific time moments, displaying amplitude variations and the visibility of defects at different phases along the time axis.

2.3. Defect Detection Using Convolutional Neural Network (CNN)

In this subsection, the methodology of interface defect detection using convolutional neural networks is described. As was shown in previous chapter, due to the systematic amplitude variations caused by the effects of sample surface and interface curvatures, traditional ultrasonic non-destructive methods cannot provide reliable interface defect detection. The development of post-processing algorithms could slightly enhance the

performance and reliability of the technique [16]; however, it could not fully eliminate the amplitude trend, keeping the detection and characterization of defects quite complex. In this particular case, though it was possible to identify all three defects in certain scans, this process required a labor-intensive examination of all scans at each time point. Such an approach is neither efficient nor practical. In contrast, convolutional neural networks offer a versatile solution, capable of recognizing complex image patterns and learning to distinguish between defective and non-defective areas, as well as variations caused by other factors.

2.3.1. Dataset Preparation

Datasets for Sample No.1 and Sample No.2 were prepared for the training, validation, and generalization of the CNN model. Two dataset classes, representing defective and non-defective areas of Sample No.1, were used for CNN training and validation. Sample No.2 was used as "unseen" data to evaluate the generalization capabilities of the model, and also had two classes of datasets. The CNN model was designed to detect defects based on ultrasound C-scans at each time point within a selected time interval, which captured a sufficient amount of data for training. This interval extended from the first interface reflection to the point where the reflections were attenuated. It included eleven multiple reflections for Sample No.1, and five for Sample No.2.

To extract the required images, C-scan generation was performed for each time moment. In total, 1906 images were generated, equally divided between two classes: defective and non-defective. Then, the dataset was divided into training and validation sets such that 70% of the data was used for CNN model training, while the remaining 30% was allocated for validation. In the case of the "unseen" data, all generated C-scans were used for validation and generalization testing. As a result, 667 images with defects and 667 without defects were used for training, while 286 defective and 286 non-defective images were set aside for validation and generalization. Examples of the C-scan images for both samples, which were used as inputs for the neural network, are presented in Figure 6.

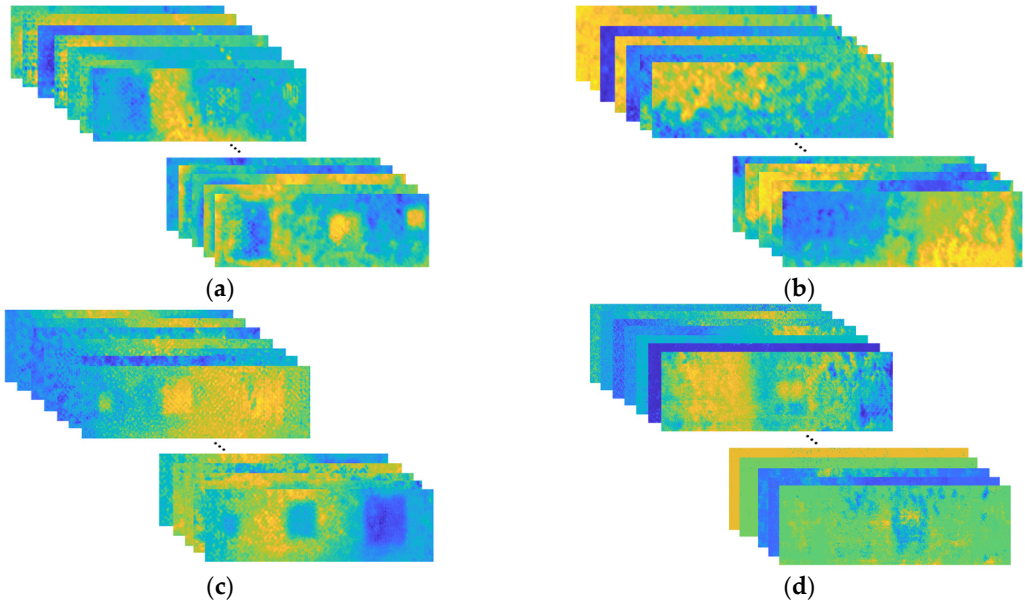

Figure 6. C-scan generation of 2 classes of datasets. (**a**) Sample No.1 "defective" area; (**b**) Sample No.1 "non-defective" area; (**c**) Sample No.2 "defective" area; (**d**) Sample No.2 "non-defective" area. colors in the image represent the amplitude of the reflected ultrasonic signals.

2.3.2. Description of the CNN

In this work, the VGG-16 convolutional neural network (CNN) architecture, developed by the Visual Geometry Group (VGG) at Oxford University in 2014 [29,30], was employed

to classify defective and non-defective areas at the interface of adhesively bonded materials, using C-scan images generated at subsequent time instances of the ultrasonic signals. The VGG-16 CNN architecture was selected for its simplicity and effectiveness in image classification tasks. The network is characterized by its use of 3 × 3 convolutional filters, which not only simplify the network design but also enhance its capacity to capture fine spatial features in images while maintaining computational efficiency. This is particularly crucial in the analysis of ultrasonic images, where defects may introduce subtle variations that require precise detection. Although more advanced architectures such as ResNet and Inception were considered for their innovative features—like skip connections and varying filter sizes within each layer—the sequential structure of VGG-16 was found to be sufficiently robust for this specific task. Additionally, VGG-16 strikes an optimal balance between accuracy and computational complexity, making it particularly well-suited for applications with limited training data, such as in non-destructive testing.

2.3.3. Training and Validation of the CNN

In this study, RGB C-scan images, encompassing both defect-free and defective cases, each with dimensions of 313 × 125 pixels, were used for training and validation. The model comprised 88,131,394 trainable parameters. The architecture of the VGG-16 network used in this study is illustrated in Figure 7.

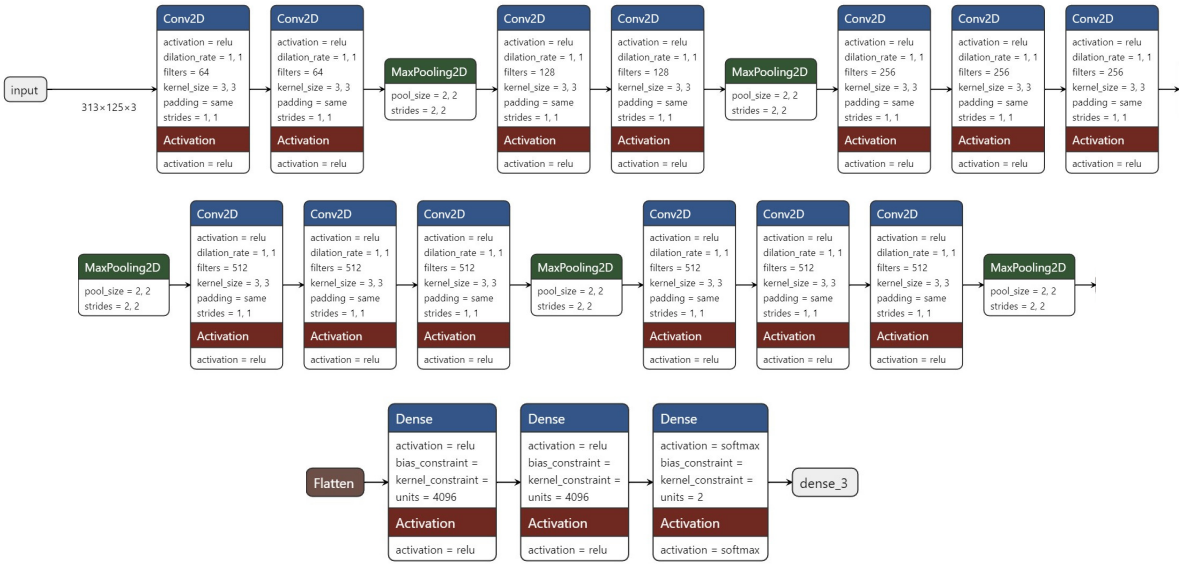

Figure 7. Architecture of the VGG-16 neural network used for classification of defects in C-scan images.

The sequential VGG-16 architecture used in this study consisted of the following layers:

- Two convolutional layers with 64 channels, 3 × 3 kernel size, and ReLU activation;
- One max-pooling layer with 2 × 2 pool size and 2 × 2 stride;
- Two convolutional layers with 128 channels, 3 × 3 kernel size, and ReLU activation;
- One max-pooling layer with 2 × 2 pool size and 2 × 2 stride;
- Three convolutional layers with 256 channels, 3 × 3 kernel size, and ReLU activation;
- One max-pooling layer with 2 × 2 pool size and 2 × 2 stride;
- Three convolutional layers with 512 channels, 3 × 3 kernel size, and ReLU activation;
- One max-pooling layer with 2 × 2 pool size and 2 × 2 stride;
- Three convolutional layers with 512 channels, 3 × 3 kernel size, and ReLU activation;
- One max-pooling layer with 2 × 2 pool size and 2 × 2 stride;
- Two fully connected (Dense) layers with 4096 units each;
- One Dense Softmax layer with two units for binary classification (defect/no-defect).

The model was trained using the Adam optimizer with a learning rate of 0.0000015, and categorical cross-entropy was selected as the loss function to evaluate probabilistic

outputs. The model was set to be trained for 50 epochs with 30 steps per epoch and 10 validation steps. Convergence was observed after 22 epochs, as the validation accuracy plateaued in the last 10 epochs without further improvement. The obtained model accuracy and validation losses are presented in Figure 8.

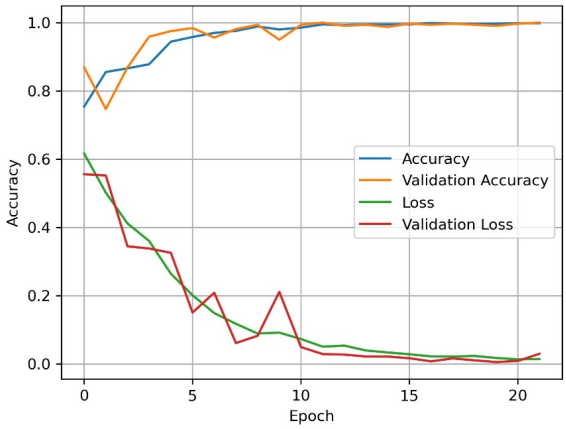

Figure 8. The obtained neural network accuracy and losses after 22 epochs of training and validation.

The model's training accuracy and losses, as shown in Figure 8, demonstrate a clear progression throughout the training process. At the initial epoch (epoch 0), the model achieved an accuracy of 0.75, with a validation loss of 0.55. By the 5th epoch, validation loss had improved to 0.33, while accuracy increased to 0.94. This upward trend continued, and by the 22nd epoch, the model reached a validation loss of 0.02 and an accuracy of 0.99.

3. Results and Discussion

Adhesively bonded lap joints of aluminum and CFRP with disbond-type defects were investigated using an ultrasonic NDT method integrated with a CNN. The primary objective of this study was to improve the performance of the traditional ultrasonic pulse-echo inspection method for detecting interface defects in adhesive bonded joints, which are influenced by surface curvature that is not visually observable. The impact of this curvature cannot be fully eliminated using traditional inspection and processing methods and significantly affects defect detection. Another goal was to automate the process to reduce the time required for investigation and analysis. Therefore, the VGG-16 convolutional neural network was utilized in conjunction with the pulse-echo ultrasonic method.

The integration of the VGG-16 CNN with the pulse-echo ultrasonic method not only improved defect detection but also allowed for automation of the entire workflow. Data preprocessing involved filtering and aligning signals by surface reflection, followed by the automatic extraction of multiple C-scan images at different time instances and training the VGG-16 network. This automation replaced manual feature extraction and data analysis, significantly reducing the time required for inspection.

We started from the main challenge, which involved systematic amplitude variations that complicate interface defect detection. To address this, C-scan images were generated at specific time moments, capturing variations over time. By automating the extraction of C-scan images at specific time moments and feeding them into the CNN, the need for manual examination by an operator was eliminated, greatly reducing the time and effort required to analyze the data. The CNN was able to process large amounts of data and classify regions as defective or non-defective with minimal operator intervention. The VGG-16 network was chosen for its ability to learn and recognize complex patterns and non-linear relationships from these images. The neural network model was tested using the validation data used in the model training process and using the unseen data, acquired from Sample No. 2 (through the independent experiment, as described in Section 2.1). The datasets were then fed into the neural network, and training was performed using the

Adam optimizer. Once trained, the VGG-16 model was capable of analyzing thousands of C-scan images quickly and efficiently, avoiding time-consuming manual interpretation. The results, including the train/validation performance and results for the "unseen" data, are presented in the confusion matrix **C**. The matrix consists of the following components: $\mathbf{C_{0,0}}$ for true positive, $\mathbf{C_{1,0}}$ for false positive, $\mathbf{C_{1,1}}$ for true negative, and $\mathbf{C_{0,1}}$ for false negative. These values correspond to the accuracy of correctly and incorrectly classified observations. Thus, the model's classification accuracy, generalization capabilities, and ability to detect subtle variations in defective and non-defective areas were assessed.

The results of "defective" versus "non-defective" classifiers of the trained VGG-16 model are presented in Figure 9.

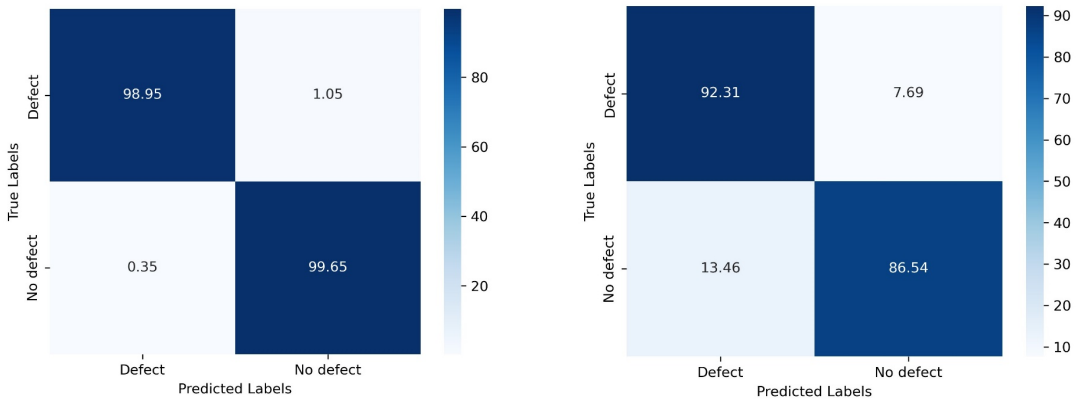

Figure 9. Confusion matrices of "defective" and "non-defective" classification using the VGG-16 model. (**a**) Confusion matrix for the train/validation data; (**b**) Confusion matrix for predictions on "unseen" experimental data.

The results presented in Figure 9a demonstrate that the model correctly identified 98.95% of true positive cases, accurately detecting the presence of defects, and 99.65% of true negative cases, where the model correctly classified the absence of defects, indicating a perfect bond. The false negative rate (defect oversight) was 1.05%, and the false positive rate (defect overestimation) was 0.35% on the training data, indicating a high level of precision and reliability during the training phase. When applied to the "unseen" dataset (Figure 9b), the model's performance slightly declined, with the true positive rate dropping to 92.31% and the true negative rate to 86.54%. Consequently, 13.46% of samples were incorrectly classified as defective, while 7.69% of actual defects were missed (classified as non-defective). While this represents a reduction in both sensitivity and specificity, it is important to consider that the training dataset was relatively limited, and the unseen data was acquired from a different sample with varying alumina and CFRP thicknesses. The unseen sample, sourced from a different manufacturer to the first sample, i.e., FL Technics in Lithuania, was specifically chosen to represent a different manufacturing process and adhesive bonding conditions compared to the Sample No.1 manufactured in COTESA GmbH, Mittweida, Germany. The unseen sample allowed us to simulate the variability in sample and bonded plate dimensions, defect sizes, environmental conditions, and interface patterns. This variability in the unseen sample reflects the range of conditions that may be encountered in real-world applications, enhancing the model's relevance and applicability in practical scenarios. Given these factors, the model's generalization and prediction capacity can be regarded as reasonably strong, particularly since both false positive and false negative rates remained within 15%, a threshold generally considered acceptable in many practical applications. Although the model showed an overall decrease in sensitivity and specificity when applied to unseen data, it is noteworthy to mention that the false positive rate (13.46%) was higher than the false negative rate (7.69%). This is generally considered favorable, as the model tends to overestimate non-defective cases as defects

rather than miss actual defects, an important quality in safety-critical industries, where overlooking defects can pose significant risks.

In addition to the confusion matrix presented in Figure 9, further performance metrics were calculated to provide a more comprehensive evaluation of the VGG-16 model's effectiveness. The accuracy, precision, recall, and F1-scores obtained on the test and unseen data are presented in Table 1.

Table 1. Additional performance metrics on the test and unseen data.

Performance Metrics	Test Data	Unseen Data
Accuracy	0.99	0.89
Precision	0.98	0.92
Recall	0.99	0.87
F1-score	0.99	0.89

While the model's performance decreased in response to unseen data, its tendency to err on the side of caution by overestimating defects rather than missing them makes it well-suited for applications where safety is a primary concern. To further improve its performance, especially in handling borderline cases, several strategies can be considered. Firstly, fine-tuning the decision threshold, or applying cross-validation and regularization techniques, may help achieve a better balance between sensitivity and specificity, allowing for a more favorable trade-off between minimizing missed defects and controlling the overestimation of defects. Secondly, enhancing the training dataset with more diverse samples could significantly improve the model's robustness and generalization. Including data from samples with varying thicknesses, different experimental conditions, and diverse defect characteristics would provide the model with a broader range of scenarios, enabling it to handle unseen data even more effectively.

4. Conclusions

In this study, an ultrasonic pulse-echo method integrated with the AGG-16 convolutional neural network was developed to detect defects in adhesive bonds and to automate the process. In the post-processing step of the collected experimental data, where the signals were aligned according to the surface reflection time, the surface curvature factor influencing the detection was reduced. However, the systematic amplitude variation at the interface remained and could not be fully mitigated. Therefore, a significant improvement in defect detection accuracy was achieved by integrating the VGG-16 CNN. The results obtained showed that the VGG-16 CNN was able to effectively learn and recognize complex patterns in the C-scan images, demonstrating its capability to adapt to non-ideal inspection conditions and automate the entire process reducing the time required. The main results of the using the VGG-16 network to classify defective and non-defective areas are as follows:

1. The VGG-16 model provided a high classification accuracy rate of 98.95% for true positive cases and 99.65% for true negative cases on the training dataset, indicating a strong ability to distinguish between defective and non-defective adhesive bonds;
2. Low false positive and negative rates were obtained during model training, at 1.05% and 0.35%, respectively, indicating a high level of precision and reliability;
3. Robust performance of the model was achieved when trialed on "unseen" data, highlighting its potential for generalization across different samples. Although the model's performance slightly declined with unseen data, its reliable classification ability was demonstrated with true positive and true negative rates of 92.31% and 86.54%, respectively;
4. The false positive and negative rates obtained on the "unseen" data remained within 15%, equaling 13.46% and 7.69%, respectively, which is still reasonably strong and acceptable in many practical applications;

5. The tendency to overestimate non-defective cases as defects rather than miss actual defects makes the model well-suited to applications where safety is paramount.

As a result, this study demonstrates that the integration of advanced neural network techniques with traditional ultrasonic inspection methods can significantly enhance detection capabilities within adhesive bonds, providing a valuable tool for ensuring the integrity and safety of critical structural components.

Author Contributions: Conceptualization, V.S. and E.J.; methodology, V.S., E.J. and D.S.; software, V.S. and D.S.; validation, V.S.; formal analysis, V.S. and D.S.; investigation, V.S., E.J. and D.S.; resources, V.S., E.J. and D.S.; data curation, D.S. and V.S.; writing—original draft preparation, D.S. and V.S.; writing—review and editing, E.J. and V.S.; visualization, D.S. and V.S.; supervision, V.S. and E.J.; project administration, V.S. and E.J.; funding acquisition, D.S. All authors have read and agreed to the published version of the manuscript.

Funding: This research was funded by the Research Council of Lithuania (LMTLT), agreement no. S-PD-22-25 and agreement no. S-MIP-22-5.

Institutional Review Board Statement: Not applicable.

Informed Consent Statement: Not applicable.

Data Availability Statement: The data presented in this study are available on request from the corresponding author. The data are not publicly available due to privacy.

Conflicts of Interest: The authors declare no conflicts of interest.

References

1. Rao, J.; Yang, F.; Mo, H.; Kollmannsberger, S.; Rank, E. Quantitative reconstruction of defects in multi-layered bonded composites using fully convolutional network-based ultrasonic inversion. *J. Sound Vib.* **2023**, *542*, 117418. [CrossRef]
2. Jasiūnienė, E.; Yilmaz, B.; Smagulova, D.; Bhat, G.A.; Cicėnas, V.; Žukauskas, E.; Mažeika, L. Non-Destructive Evaluation of the Quality of Adhesive Joints Using Ultrasound, X-ray, and Feature-Based Data Fusion. *Appl. Sci.* **2022**, *12*, 2930. [CrossRef]
3. Smagulova, D.; Yilmaz, B.; Jasiuniene, E. Ultrasonic Features for Evaluation of Adhesive Joints: A Comparative Study of Interface Defects. *Sensors* **2024**, *24*, 176. [CrossRef] [PubMed]
4. Jodhani, J.; Handa, A.; Gautam, A.; Ashwni; Rana, R. Ultrasonic non-destructive evaluation of composites: A review. *Mater. Today Proc.* **2023**, *78*, 627–632. [CrossRef]
5. Tunukovic, V.; McKnight, S.; Pyle, R.; Wang, Z.; Mohseni, E.; Gareth Pierce, S.; Vithanage, R.K.W.; Dobie, G.; MacLeod, C.N.; Cochran, S.; et al. Unsupervised machine learning for flaw detection in automated ultrasonic testing of carbon fibre reinforced plastic composites. *Ultrasonics* **2024**, *140*, 107313. [CrossRef]
6. Spytek, J.; Ambrozinski, L.; Pieczonka, L. Evaluation of disbonds in adhesively bonded multilayer plates through local wavenumber estimation. *J. Sound Vib.* **2022**, *520*, 116624. [CrossRef]
7. Solodov, I.; Kornely, M.; Philipp, J.; Stammen, E.; Dilger, K.; Kreutzbruck, M. Linear vs nonlinear ultrasonic testing of kissing bonds in adhesive joints. *Ultrasonics* **2023**, *132*, 106967. [CrossRef]
8. Angiulli, G.; Calcagno, S.; De Carlo, D.; Lagana, F.; Versaci, M. Second-order parabolic equation to model, analyze, and forecast thermal-stress distribution in aircraft plate attack wing-fuselage. *Mathematics* **2020**, *8*, 6. [CrossRef]
9. Fan, Z.; Bai, K.; Chen, C. Ultrasonic testing in the field of engineering joining. *Int. J. Adv. Manuf. Technol.* **2024**, *132*, 4135–4160. [CrossRef]
10. Chen, L.; Zhang, Y.; Xie, J.; Liu, P.; Han, Y.; Liu, R.; Xu, C.; Song, G. Simultaneous inspection of multi-kind defects in adhesively bonded CFRP/steel structures by inductive thermography. *Infrared Phys. Technol.* **2024**, *138*, 105254. [CrossRef]
11. Chen, H.; Tao, J. Utilizing improved YOLOv8 based on SPD-BRSA-AFPN for ultrasonic phased array non-destructive testing. *Ultrasonics* **2024**, *142*, 107382. [CrossRef] [PubMed]
12. Yılmaz, B.; Jasiūnienė, E. Advanced ultrasonic NDT for weak bond detection in composite-adhesive bonded structures. *Int. J. Adhes. Adhes.* **2020**, *102*, 102675. [CrossRef]
13. Yi, Q.; Tian, G.Y.; Yilmaz, B.; Malekmohammadi, H.; Laureti, S.; Ricci, M.; Jasiuniene, E. Evaluation of debonding in CFRP-epoxy adhesive single-lap joints using eddy current pulse-compression thermography. *Compos. Part B Eng.* **2019**, *178*, 107461. [CrossRef]
14. Sun, H.; Kosukegawa, H.; Takagi, T.; Uchimoto, T.; Hashimoto, M.; Takeshita, N. Electromagnetic pulse-induced acoustic testing and the pulsed guided wave propagation in composite/metal adhesive bonding specimens. *Compos. Sci. Technol.* **2021**, *201*, 108499. [CrossRef]
15. Markatos, D.N.; Pantelakis, S.G.; Tserpes, K.I. The Effect of Contamination-Generated Defects on the Mechanical Performance of Adhesively Bonded Joints; Destructive and Non-Destructive Assessment. *Compr. Struct. Integr.* **2023**, *2*, 810–833. [CrossRef]

16. Smagulova, D.; Mazeika, L.; Jasiuniene, E. Novel processing algorithm to improve detectability of disbonds in adhesive dissimilar material joints. *Sensors* **2021**, *21*, 3048. [CrossRef]
17. Ghose, B.; Panda, R.S.; Balasubramaniam, K. Guided A0 wave mode interaction with interfacial disbonds in an elastic-viscoelastic bilayer structure. *NDT E Int.* **2021**, *124*, 102543. [CrossRef]
18. Rucka, M.; Wojtczak, E.; Lachowicz, J. Damage imaging in lamb wave-based inspection of adhesive joints. *Appl. Sci.* **2018**, *8*, 522. [CrossRef]
19. Santos, M.; Santos, J. Adhesive Single-Lap Joint Evaluation Using Ultrasound Guided Waves. *Appl. Sci.* **2023**, *13*, 6523. [CrossRef]
20. Yilmaz, B.; Asokkumar, A.; Jasiūnienė, E.; Kažys, R.J. Air-coupled, contact, and immersion ultrasonic non-destructive testing: Comparison for bonding quality evaluation. *Appl. Sci.* **2020**, *10*, 6757. [CrossRef]
21. Yilmaz, B.; Ba, A.; Jasiuniene, E.; Bui, H.K.; Berthiau, G. Evaluation of Bonding Quality with Advanced Nondestructive Testing (NDT) and Data Fusion. *Sensors* **2020**, *20*, 5127. [CrossRef] [PubMed]
22. Li, Y.; Yao, K.; Li, X. An ultrasonic signal reconstruction algorithm of multilayer composites in non-destructive testing. *Appl. Acoust.* **2022**, *186*, 108461. [CrossRef]
23. Lee, H.; Koo, B.; Chattopadhyay, A.; Neerukatti, R.K.; Liu, K.C. Damage detection technique using ultrasonic guided waves and outlier detection: Application to interface delamination diagnosis of integrated circuit package. *Mech. Syst. Signal Process.* **2021**, *160*, 107884. [CrossRef]
24. Tenreiro, A.F.G.; Ramalho, G.M.F.; Lopes, A.M.; da Silva, L.F.M. Structural monitoring of adhesive joints using machine learning. In *Advances in Structural Adhesive Bonding*, 2nd ed.; Elsevier: Amsterdam, The Netherlands, 2023; pp. 909–949. [CrossRef]
25. Lagana, F.; Prattico, D.; Angiulli, G.; Oliva, G.; Pullano, S.A.; Versaci, M.; La Foresta, F. Development of an Integrated System of sEMG Signal Acquisition, Processing, and Analysis with AI Techniques. *Signals* **2024**, *5*, 476–493. [CrossRef]
26. Versaci, M.; Angiulli, G.; Crucitti, P.; De Carlo, D.; Lagana, F.; Pellicano, D.; Palumbo, A. A Fuzzy Similarity-Based Approach to Classify Numerically Simulated and Experimentally Detected Carbon Fiber-Reinforced Polymer Plate Defects. *Sensors* **2022**, *22*, 4232. [CrossRef]
27. Wang, Y.; Wang, K.; Zhang, C. Applications of artificial intelligence/machine learning to high-performance composites. *Compos. Part B Eng.* **2024**, *285*, 111740. [CrossRef]
28. Smagulova, D.; Samaitis, V.; Jasiuniene, E. Machine learning based approach for automatic defect detection and classification in adhesive joints. *NDT E Int.* **2024**, *148*, 103221. [CrossRef]
29. Simonyan, K.; Zisserman, A. Very Deep Convolutional Networks for Large-Scale Image Recognition. *arXiv* **2015**. [CrossRef]
30. Cirtautas, D.; Samaitis, V.; Mažeika, L.; Raišutis, R. Detection and Classification of Uniform and Concentrated Wall-Thinning Defects Using High-Order Circumferential Guided Waves and Artificial Neural Networks. *Sensors* **2023**, *23*, 6505. [CrossRef]